



Water-induced construction of Cs₄PbBr₆/CsPbBr₃ heterojunction for efficient perovskite light-emitting diode

Jingjing Cao, Xiankan Zeng, Wen Li, Liang Lv, Cheng Yan, Haichao Huang, Jun Lu^{*}, Weiqing Yang^{*}

Key Laboratory of Advanced Technologies of Materials (Ministry of Education), School of Materials Science and Engineering, Southwest Jiaotong University, Chengdu 610031, PR China

ARTICLE INFO

Keywords:

Water
Cs₄PbBr₆/CsPbBr₃ heterojunction
Perovskite nanocrystals
Light-emitting diode

ABSTRACT

Perovskite Cs₄PbBr₆/CsPbBr₃ heterojunction with a strongly carrier-confined effect is emerging as a promising luminescent material for perovskite light-emitting diodes (PeLEDs). However, it is a big challenge to construct the heterojunction on a molecular scale to fully excavate this confinement effect for efficient electroluminescence efficiencies of PeLEDs. Herein, we report a water-induced construction of Cs₄PbBr₆/CsPbBr₃ heterojunction for efficient PeLEDs via adding trace water with strong polarity. Benefiting from its strong carrier confinement effect, this heterojunction has a higher exciton binding energy (94.7 meV) and a lower nonradiative decay rate constant (0.007 ns⁻¹) compared to that of single CsPbBr₃ nanocrystals (NCs) (14.1 meV and 0.031 ns⁻¹). Based on it, the as-fabricated PeLEDs exhibit a greatly-improved maximum current efficiency of 43.62 cd A⁻¹ and a peak EQE of 11.31%, approximately 1.5 times that of CsPbBr₃ NCs (28.43 cd A⁻¹ and 7.78%). Evidently, this work provides an important way toward the construction of Cs₄PbBr₆/CsPbBr₃ heterojunction and then promotes the commercial development of heterojunction-like optoelectronics.

1. Introduction

All inorganic lead halide perovskite (CsPbX₃, X = Cl, Br, I) nanocrystals (PNCs) with outstanding optical and electrical properties have been regarded as promising materials for photovoltaic and optoelectronic applications, such as solar cells [1–3], perovskite light-emitting diodes (PeLEDs) [4–11], laser [12,13] and photodetectors [14,15]. Among them, CsPbBr₃ NCs naturally possessing high photoluminescence quantum yields (PLQYs), narrow emission spectrum and wide tunable emission [16–18], have gained much attention for light-emitting applications. The external quantum efficiency (EQE) of CsPbBr₃-based PeLEDs has been optimized from an initial 0.12% to over 20% in just a few years [5]. However, the smaller exciton binding energies of three-dimensional (3D) CsPbBr₃ NCs at room temperature (RT) result in facile dissociation of excitons and slower radiative recombination efficiency [19–21]. Free carriers from dissociation are easily captured by nonradiative recombination centers, leading to more defect states [22, 23]. Hence, the single 3D CsPbBr₃ NCs exhibit weak defect passivation and carrier confinement capacities.

To solve this problem, the construction of heterojunction is a

potential strategy to spatially confine electrons and holes of CsPbBr₃ NCs and improve the radiative recombination efficiency. Recently, researchers have constructed Cs₄PbBr₆-CsPbBr₃ heterodimer, 3D/2D (CsPbBr₃/CsPb₂Br₅) heterojunctions, CsPbBr₃/CsPb₂Br₅ and CsPbBr₃/Cs₄PbBr₆ core/shell structures to enhance the optical performance of 3D CsPbBr₃ NCs [18,24–34]. These structures were evidently proved to effectively confine electrons and holes of CsPbBr₃ NCs for the obvious improvement of the radiative recombination efficiency [25,35]. Furthermore, these structures were also applicable to organic-inorganic hybrid perovskites, such as MAPbBr₃ and FAPbBr₃ with improved optical performance and stability [36,37]. But most of these composite structures were simply mixed or epitaxially grown, inevitably leading to a serious or slight lattice mismatch and then weakening the confinement effect. So far, it is still a big challenge to construct heterojunctions on a molecular scale to fully excavate this confinement effect for efficient electroluminescence efficiencies of PeLEDs.

Herein, we successfully construct a Cs₄PbBr₆/CsPbBr₃ heterojunction to enhance the performances of PeLEDs by adding trace water with strong polarity. Due to the strong carrier confinement effect, this heterojunction has a higher exciton binding energy (94.7 meV) and a

^{*} Corresponding authors.

E-mail addresses: Junlyuprc@hotmail.com (J. Lu), wqyang@swjtu.edu.cn (W. Yang).

<https://doi.org/10.1016/j.apmt.2023.101733>

Received 12 October 2022; Received in revised form 8 December 2022; Accepted 11 January 2023

Available online 17 January 2023

2352-9407/© 2023 Elsevier Ltd. All rights reserved.

lower nonradiative decay rate constant (0.007 ns^{-1}) compared to that of the single CsPbBr_3 NC (14.1 meV and 0.031 ns^{-1}). Furthermore, the as-fabricated PeLEDs exhibit a maximum current efficiency of 43.62 cd A^{-1} and a peak EQE of 11.31%, one of the best devices performance based on the $\text{Cs}_4\text{PbBr}_6/\text{CsPbBr}_3$ system. Therefore, this work may provide a potential path to construct $\text{Cs}_4\text{PbBr}_6/\text{CsPbBr}_3$ heterojunction for the commercial development of heterojunction-like optoelectronics.

2. Results and discussion

Water-induced construction of $\text{Cs}_4\text{PbBr}_6/\text{CsPbBr}_3$ heterojunction contains two stages: kinetically fast growth process (Stage I) and polar molecular tailoring process (Stage II). For Stage I, strong polar water can contribute to activating the PNCs surface by reducing the density of surface capping ligands [38,39]. Furthermore, some small-sized PNCs already formed can be re-dissolved by adding water and then the precursor concentration increases, generating a faster growth rate and large-sized CsPbBr_3 PNCs [38,40]. Next, the large-sized CsPbBr_3 PNCs can be transformed into $\text{Cs}_4\text{PbBr}_6/\text{CsPbBr}_3$ heterojunction via a polar molecular tailoring process. As shown in Fig. 1a, the pure CsPbBr_3 with a corner shared $[\text{PbBr}_6]^{4-}$ octahedron is surrounded by the strong polar H_2O molecular. As a polar molecular scissor, this scissor will locally tailor the shared vertices between interconnected $[\text{PbBr}_6]^{4-}$ octahedral of the CsPbBr_3 crystal. After tailoring, the CsPbBr_3 is transformed into the Cs_4PbBr_6 with isolated $[\text{PbBr}_6]^{4-}$ octahedral.

The whole water-induced construction of the $\text{Cs}_4\text{PbBr}_6/\text{CsPbBr}_3$ heterojunction could be described by the following equation:



Eventually, the lattice-matched $\text{Cs}_4\text{PbBr}_6/\text{CsPbBr}_3$ heterojunction is formed. The corresponding phase transformation from CsPbBr_3 to Cs_4PbBr_6 has also been achieved by adding ZnBr_2 [41] or prolonging exposure to humidity of CsPbBr_3 film [42]. The polar molecular tailoring process is similar to the interaction of organic-inorganic hybrid perovskites with trace water such as MAPbI_3 , accompanied by a phase transition from MAPbI_3 to $\text{MA}_4\text{PbI}_6 \cdot 2\text{H}_2\text{O}$ [43,44]. Furthermore, the lattice constant of Cs_4PbBr_6 matches well with that of CsPbBr_3 , and Cs_4PbBr_6 could effectively passivate the CsPbBr_3 surface without additional interface strain [21,24]. Herein, this heterojunction can also effectively reduce the nonradiative recombination rate and trap states. From Fig. 1b, the smaller exciton binding energy of CsPbBr_3 PNCs would undesirably lead to the separation and migration of injected charge carriers, which will dramatically reduce the number of formed excitons. In the more severe cases, the defect states in the grain boundary would trap already-formed excitons, resulting in their quenching [35,45]. These issues will seriously restrict the efficiency of the radiative recombination of PNCs. In contrast, the construction of $\text{Cs}_4\text{PbBr}_6/\text{CsPbBr}_3$ heterojunction can greatly improve the efficiency of radiative recombination (Fig. 1c), which can be attributed to two aspects: (i) the larger exciton binding energy of $\text{Cs}_4\text{PbBr}_6/\text{CsPbBr}_3$ heterojunction can make charge carriers easier to be confined into excitons (carrier confinement effect); (ii) the trap states are passivated by Cs_4PbBr_6 of $\text{Cs}_4\text{PbBr}_6/\text{CsPbBr}_3$ heterojunction, substantially reducing quenching losses [21,24].

Fig. 2 shows the morphological and structural characterization of

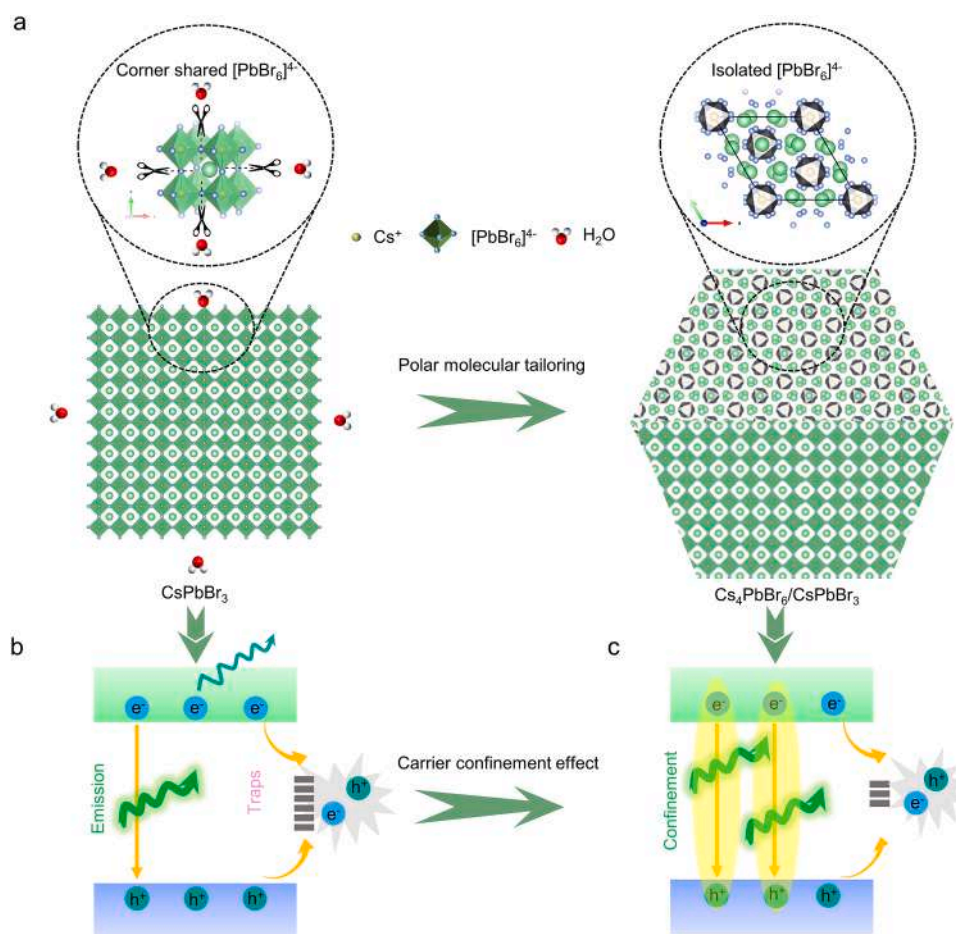


Fig. 1. Schematic illustrations of the polar molecular tailoring process. (a) Schematically showing a water-induced construction of $\text{Cs}_4\text{PbBr}_6/\text{CsPbBr}_3$ heterojunction. Schematic illustrations of (b) charge migration and nonradiative recombination, (c) carrier confinement and trap passivation processes.

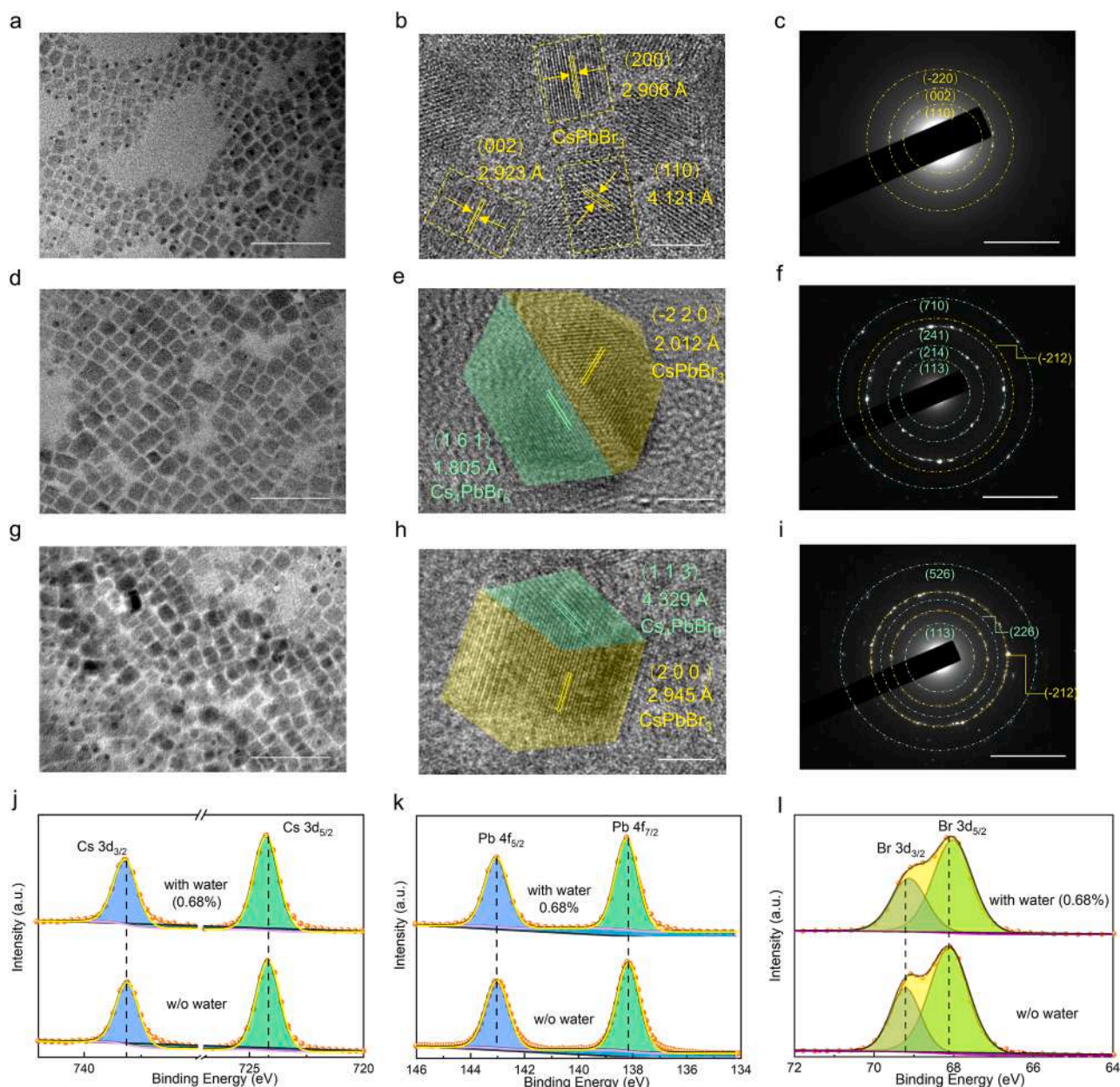


Fig. 2. Morphological and structural characterization. TEM images of (a) CsPbBr₃ (w/o water), (d) Cs₄PbBr₆/CsPbBr₃ heterojunction (with water: 0.68%) and (g) Cs₄PbBr₆/CsPbBr₃ heterojunction (with water: 1.36%). The scale bar is 50 nm. HR-TEM images of (b) CsPbBr₃ (w/o water), (e) Cs₄PbBr₆/CsPbBr₃ heterojunction (with water: 0.68%) and (h) Cs₄PbBr₆/CsPbBr₃ heterojunction (with water: 1.36%). The scale bar is 5 nm. Cs₄PbBr₆ domains are shaded in green, and CsPbBr₃ domains are shaded in yellow; SAED patterns of (c) CsPbBr₃ (w/o water), (f) Cs₄PbBr₆/CsPbBr₃ heterojunction (with water: 0.68%) and (i) Cs₄PbBr₆/CsPbBr₃ heterojunction (with water: 1.36%). The scale bar is 5 nm⁻¹. The yellow circle represents the CsPbBr₃ phase, and the cyan circle represents the Cs₄PbBr₆ phase. (j–l) XPS spectra of Cs 3d (j), Pb 4f (k) and Br 3d (l) of the PNCs with (0.68% water) and w/o water.

CsPbBr₃ without (w/o) water and Cs₄PbBr₆/CsPbBr₃ heterojunction (with water: 0.68% and 1.36%). In Figs. 2a, 2d, 2g and S1a–c, the average lateral dimension of PNCs with water (10.86 nm for 0.68% water, 10.21 nm for 1.36% water) is much larger than that of PNCs w/o water (7.07 nm). This is attributed to the water-induced particle size increase of PNC [38] and a result of the kinetically fast growth process (Stage (I)). From their HRTEM images, the PNCs w/o water present characteristic interplanar spacing of 2.906 Å, 2.923 Å and 4.121 Å, assigned to (2 0 0), (0 0 2) and (1 1 0) crystal faces of CsPbBr₃, respectively, identifying the formation of pure CsPbBr₃ phase (Fig. 2b). While except for (-2 2 0) and (2 0 0) crystal faces of CsPbBr₃ phase, PNCs with water also show the interplanar spacing of 1.805 Å and 4.329 Å attributed to (1 6 1) and (1 1 3) crystal faces of Cs₄PbBr₆ phase

(Fig. 2e, 2h). These results evidently prove the construction of Cs₄PbBr₆/CsPbBr₃ heterojunction on a molecular scale with the addition of water. Moreover, the lattice mismatch is also calculated. For the PNCs with 0.68% water, the lattice mismatch is 2.53% between the (2 0 2) plane of CsPbBr₃ [$7d_{202}$ (CsPbBr₃) = 14.084 Å] and (1 6 1) plane of Cs₄PbBr₆ [$8d_{113}$ (Cs₄PbBr₆) = 14.44 Å]. And a mismatch of 2.00% between $2d_{113}$ (Cs₄PbBr₆) = 8.658 Å and $3d_{200}$ (CsPbBr₃) = 8.835 Å is obtained for Cs₄PbBr₆/CsPbBr₃ PNCs with 1.36% water. This slight mismatch is lower than 5% in the published reports [25,31,33], indicating excellent lattice matching for water-induced construction of Cs₄PbBr₆/CsPbBr₃ heterojunction.

The corresponding selected area electron diffraction patterns (SAED) in Fig. 2c, 2f and 2i also confirm the formation of Cs₄PbBr₆/CsPbBr₃

heterojunction for the PNCs with water. As shown in Fig. S2, PNC w/o water is the monoclinic CsPbBr₃ phase, while PNC with 0.68% or 1.36% water is the mixed phase of CsPbBr₃/Cs₄PbBr₆, which further confirms the formation of Cs₄PbBr₆/CsPbBr₃ heterojunction. These XRD results are well consistent with their HRTEM and SAED results. Moreover, X-ray photoelectron spectroscopy (XPS) quantitative analysis of PNCs with and w/o water show significantly-improved ratios of Cs/Pb (0.99~1.01) and Br/Pb (3.07~4.36) of PNCs with water (0.68%), reconfirming the coexistence of Cs₄PbBr₆ and CsPbBr₃ phases (Fig. S3). In Fig. 2j, 2k, compared with PNCs w/o water, the Cs 3d and Pb 4f peaks of PNCs with water slightly shift to a higher binding energy, manifesting that H₂O molecular indeed attaches to the PNCs surface via coordination with Cs⁺ and Pb²⁺ [38,46]. While for Br 3d peak, the lower binding energy obviously reveals the weaker Pb-Br bonding of adjacent [PbBr₆]⁴⁻ octahedra from Cs₄PbBr₆/CsPbBr₃ heterojunction (Fig. 2l), which is in good agreement with TEM and XRD results. Therefore, the Cs₄PbBr₆/CsPbBr₃ heterojunction is successfully constructed by adding water.

Fig. 3 further confirms the water-induced construction of Cs₄PbBr₆/CsPbBr₃ heterojunction from the photophysical perspective. In Fig. 3a and Table S1, PNCs with water have a lower Urbach energy (E_u) (41.1 meV) from their absorption spectra (the detailed analysis in Figs. S4 and S5) compared to that of w/o water (45.0 meV), revealing the fewer defect states of Cs₄PbBr₆/CsPbBr₃ heterojunction. As shown in Fig. 3b, the steady-state photoluminescence (PL) peaks of PNCs change from 504 nm (w/o water) to 515 nm (with water), showing an obvious red-shift consistent with the absorption spectra (Figs. S4 and S5). The red shift of the emission peak is due to the formation of the large-sized PNCs (Fig. S2). To further analyze the energy band structure of Cs₄PbBr₆/CsPbBr₃ heterojunction, the calculated valence band potential ($E_{VB, XPS}$) is 2.312 eV for CsPbBr₃ and 2.770 eV for Cs₄PbBr₆, respectively (Fig. S6). The corresponding standard hydrogen electrode ($E_{VB, NHE}$) is estimated to be 2.072 eV for CsPbBr₃ and 2.570 eV for Cs₄PbBr₆ [47].

The conduction band (CB) potential can be obtained by the sum of the bandgap and $E_{VB, NHE}$. Based on the above calculation results, the constructed Cs₄PbBr₆/CsPbBr₃ heterojunction belongs to a type I heterojunction, where both electrons and holes are confined in the CsPbBr₃ due to the barrier effect of Cs₄PbBr₆ with a wide band gap (Fig. S7) [48].

As illustrated in Fig. 3c, compared with PNCs w/o water, the PNCs with water exhibit a stronger green emission, a higher photoluminescence quantum yield (PLQY) and a narrower full-width at half-maximum (FWHM), indicating an enhanced PL performance (Table S1). The corresponding Commission Internationale de l'Eclairage (CIE) coordinates of PNCs are shown in Fig. S8 and Table S1. To better understand the role of Cs₄PbBr₆/CsPbBr₃ type I heterojunction on the charge carrier dynamics, time-resolved PL (TRPL) decay measurements are conducted. From Fig. 3d, the average PL lifetime (τ_{ave}) for the PNCs with water is 20.778 ns, 2.2 times higher than that of the PNCs w/o water (9.383 ns) fitted by bi-exponential function, identifying reduced trap states (Table S2) [37]. Furthermore, the PNCs with water possess a much slower nonradiative decay rate constant (K_{nr}) of 0.007 ns⁻¹ compared to that of 0.031 ns⁻¹ for PNCs w/o water (Table S2), fully revealing enhanced radiation recombination and reduced trap states for Cs₄PbBr₆/CsPbBr₃ type I heterojunction [49].

In general, the radiative recombination efficiency is supposed to be relevant to the exciton binding energy (E_b) [50]. So the temperature-dependent PL spectra (80 ~ 300 K) measurements were executed in Fig. S9. Both the PL spectra of PNCs with and w/o water show a continuous blue-shift and the gradually-decreased PL intensity with increasing temperature, which is ascribed to the increased probability of nonradiative recombination process caused by thermal activation [36]. In Fig. 3e, the calculated E_b of PNCs w/o water fitted by the Arrhenius equation [51] is only 14.1 meV, much lower than RT thermal ionization energy (26 meV), so the excitons for CsPbBr₃ at RT are easy to ionize to free excitons [52], resulting in a lower radiative recombination efficiency. In comparison, PNCs with water have a larger E_b of 94.7 meV,

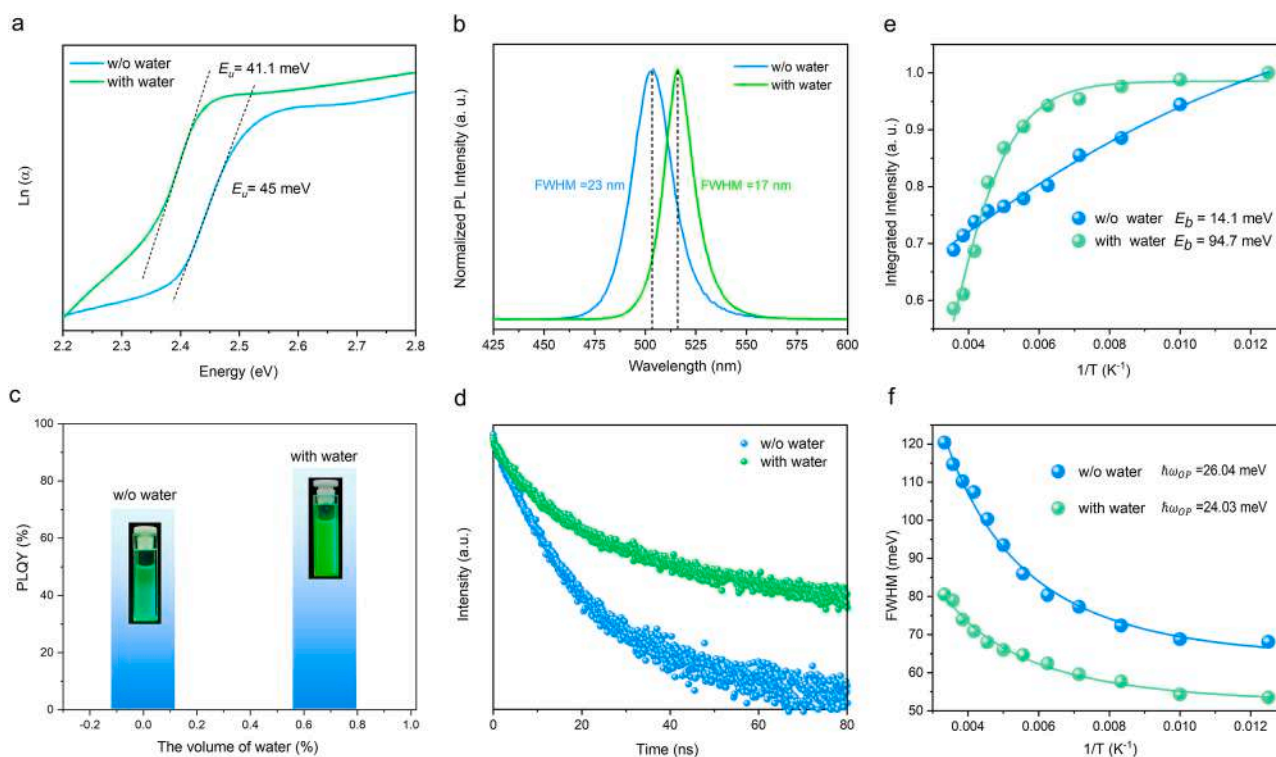


Fig. 3. Photophysical properties characterization analysis. (a) Urbach energy (E_u) diagram for the PNCs with and w/o water. (b) Normalized steady-state photoluminescence (PL) spectra and (c) photoluminescence quantum yield (PLQY) of PNCs with and w/o water. Inset: The photographs of PNCs w/o and with water under UV light. (d) Time-resolved PL spectra. (e) Temperature-dependent integrated PL intensity and (f) PL full-width at half-maximum (FWHM) as a function of reciprocal temperature in the range from 80 K to 300 K.

approaching previous reports [4,36], nearly seven times as much as that of PNCs w/o water. This result evidently manifests the stronger confinement effect of $\text{Cs}_4\text{PbBr}_6/\text{CsPbBr}_3$ type I heterojunction. As shown in Fig. 3f, the optical phonon energy ($\hbar\omega_{OP}$) are derived by adapting the independent Boson model [51]. The fitted value of $\hbar\omega_{OP}$ for PNC with water is 24.03 meV, lower than that of PNC w/o water (26.04 meV), indicating reduced carrier-phonon coupling for the $\text{Cs}_4\text{PbBr}_6/\text{CsPbBr}_3$ type I heterojunction. This optical phonon energy result agrees well with the value of $\hbar\omega_{OP}$ (16–40 meV) [53]. Therefore, this $\text{Cs}_4\text{PbBr}_6/\text{CsPbBr}_3$ type I heterojunction has a slower nonradiative recombination rate and a lower trap state, which will be a potential candidate for fabricating high-performance PeLEDs.

Photo, thermal and water stabilities are important indicators to evaluate the PL performance of PNCs for LED applications. Fig. 4 presents the corresponding stability characterizations. Compared with PNCs w/o water, the PL intensity of PNCs with water is almost unchanged under continuous ultraviolet radiation (UV) for 3 h (Fig. 4a–c). In Fig. 4d, 4e, the PL intensity of PNCs w/o water exhibit an obvious decrease along with a slight red-shift of the PL spectrum, while the PNCs with water maintain 70% of initial PL intensity with constant PL emission peak when the temperature reaches 140 °C (Fig. 4f). In Fig. 4g–i, the

PL intensity of PNCs with water have a smaller decrease accompanied by the slight red-shift of PL spectrum than that of PNCs w/o water over time. Therefore, these stability measurement results fully signify that $\text{Cs}_4\text{PbBr}_6/\text{CsPbBr}_3$ type I heterojunction should tremendously boost the photo, heat and water stabilities of PNCs and greatly facilitate the commercialization development of PeLEDs.

Finally, we fabricated PeLED devices using a layered structure of ITO/PEDOT: PSS/PTAA/PNCs/TPBi/LiF/Al, as illustrated in Fig. 5a. The VB of PNCs with water is determined by the ultraviolet photoelectron spectroscopy and the CB is the sum of VB and band gap (Fig. S10). From Fig. 5b, the EL spectra of PNCs with water show a constant EL peak located at 518 nm with an increased EL intensity as the bias voltage increase (3 V - 6 V). The inset of Fig. 5b shows a bright green emission of the device under an operation voltage of 6 V. As presented in Fig. 5c, the maximum luminance of PeLED devices using PNCs with water (50,221 cd m^{-2}) is approximately 3 times that of PNCs w/o water (16,780 cd m^{-2}). From Fig. 5d, PeLED devices based on PNCs with water exhibit the highest current efficiency (CE) of 43.62 cd A^{-1} and a peak EQE of 11.31%, much higher than that of PNCs w/o water (28.43 cd A^{-1} and 7.78%). Furthermore, as shown in Fig. S11, PeLEDs with water exhibit a superior T_{50} (indicating the time that the luminance decreased to 50% of

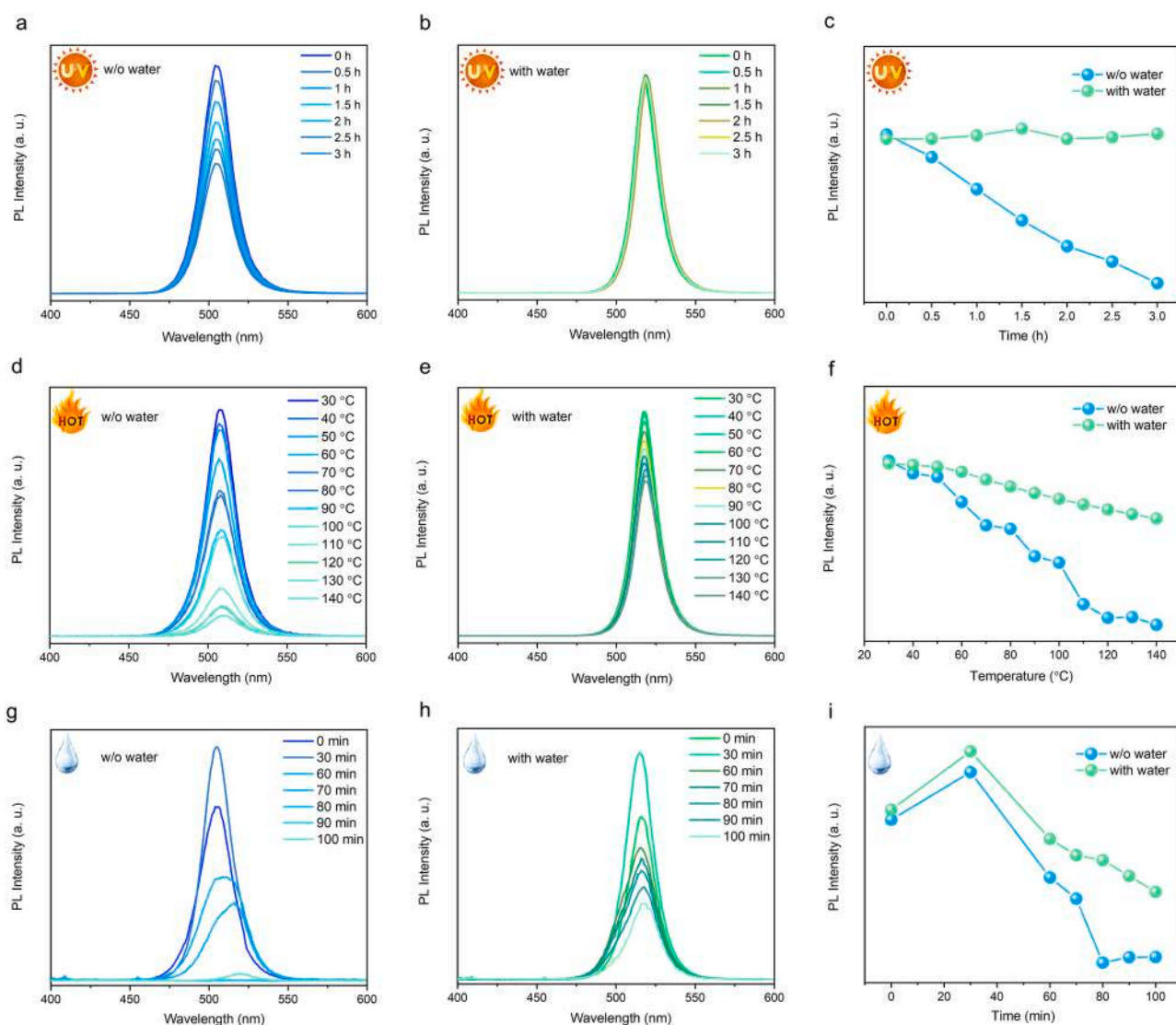


Fig. 4. Environmental stability test. PL spectra of PNCs with (a) and w/o water (b). (c) The time-dependent PL intensity under continuous ultraviolet (UV) radiation (365 nm , 5 mW cm^{-2}). PL spectra of PNCs with (d) and w/o water (e). (f) PL intensity as a function of temperature at $30 \sim 140 \text{ }^\circ\text{C}$. PL spectra of PNCs with (g) and w/o water (h). (i) PL intensity with water treatment time.

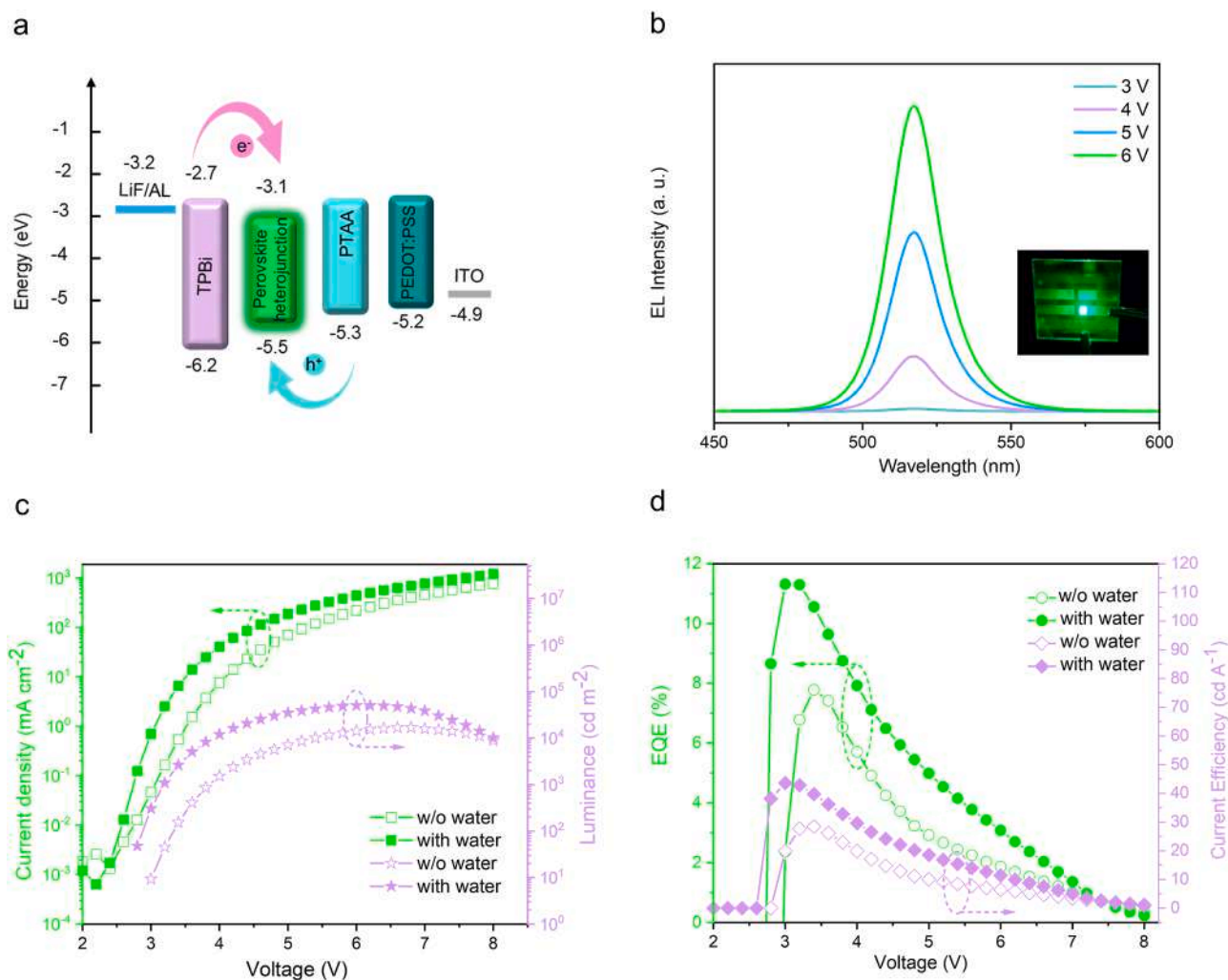


Fig. 5. Device performance of PeLEDs. (a) Energy-level diagram of the PeLED device structure. (b) EL spectra of the PeLED device of PNCs with water under 3 V-6 V. Inset showed a photograph at an operation voltage of 6 V. (c) Current density -luminance-voltage curves of PLED devices. (d) EQE-current efficiency- voltage curves of PLED devices.

the initial value) of 135 min, much longer than that of PeLEDs w/o water (86 min). The detailed EL performances of PeLED devices fabricated by PNCs with water are summarized in Table S3. The enhanced EL performances demonstrate the superiority of *in-situ* constructing $\text{Cs}_4\text{PbBr}_6/\text{CsPbBr}_3$ heterojunction, which is one of the best devices performance based on the $\text{Cs}_4\text{PbBr}_6/\text{CsPbBr}_3$ system (Table S4).

3. Conclusions

In summary, we reported water-induced construction of $\text{Cs}_4\text{PbBr}_6/\text{CsPbBr}_3$ heterojunction for efficient PeLEDs. This heterojunction possesses significantly enhanced PLQY, PL lifetime and exciton binding energy, which should be attributed to the enhanced radiation recombination and reduced trap states. Furthermore, the PNCs with water exhibited improved photo, heat and water stabilities. Based on this $\text{Cs}_4\text{PbBr}_6/\text{CsPbBr}_3$ heterojunction, the fabricated PeLED device exhibits a maximum current efficiency of 43.62 cd A^{-1} and a peak EQE of up to 11.31%, much higher than that of CsPbBr_3 PNCs. Therefore, this work may provide a promising strategy for constructing $\text{Cs}_4\text{PbBr}_6/\text{CsPbBr}_3$ heterojunction on a molecular scale and promote the commercial development of heterojunction-like optoelectronics.

CRediT authorship contribution statement

Jingjing Cao: Conceptualization, Methodology, Investigation, Writing – original draft, Writing – review & editing. **Xiankan Zeng:** Resources, Investigation. **Wen Li:** Writing – original draft, Visualization, Funding acquisition. **Liang Lv:** Resources, Supervision. **Cheng Yan:** Resources, Supervision. **Haichao Huang:** Resources, Supervision. **Jun Lu:** Project administration, Funding acquisition. **Weiqing Yang:** Resources, Writing – review & editing, Supervision, Funding acquisition.

Declaration of Competing Interest

The authors declare that they have no known competing financial interests or personal relationships that could have appeared to influence the work reported in this paper.

Data availability

Data will be made available on request.

Acknowledgments

This work was financially supported by the National Natural Science

Foundation of China (No. 52073237), by Young Scientific and Technological Innovation Research Team Funds of Sichuan Province (No. 20CXTD0106 and 2019YFG0292) and by Fundamental Research Funds for the Central Universities (No. 2682020CX06). The first author is very grateful to her husband, Mr. Chen. We are thankful to the Analytical and Testing Center of Southwest Jiaotong University for supporting the XRD and TEM measurements.

Supplementary materials

Supplementary information file contains experimental section, tables with the summary of PL performances, TRPL parameters performances of the PeLED device and EL properties of CsPbBr₃-based heterojunction PLED devices, and extra figures with the size distribution histograms, XRD patterns, surface atomic ratio analysis, UV–vis absorption spectra, Tauc plots, VB-XPS plots, energy band diagram of Cs₄PbBr₆/CsPbBr₃ type I heterojunction, CIE coordinates, temperature-dependent PL spectra, UPS data and the operational stability of PLEDs.

Supplementary material associated with this article can be found, in the online version, at doi:10.1016/j.apmt.2023.101733.

References

- J. Lin, M. Lai, L. Dou, C.S. Kley, H. Chen, F. Peng, J. Sun, D. Lu, S.A. Hawks, C. Xie, F. Cui, A.P. Alivisatos, D.T. Limmer, P. Yang, Thermochromic halide perovskite solar cells, *Nat. Mater.* 17 (3) (2018) 261–267, <https://doi.org/10.1038/s41563-017-0006-0>.
- A. Swarnkar, A.R. Marshall, E.M. Sanehira, B.D. Chernomordik, D.T. Moore, J. A. Christians, T. Chakrabarti, J.M. Luther, Quantum dot-induced phase stabilization of α -CsPbI₃ perovskite for high-efficiency photovoltaics, *Science* 354 (6308) (2016) 92–95, <https://doi.org/10.1126/science.aag2700>.
- D. Forgács, L. Gil-Escrig, D. Pérez-Del-Rey, C. Mombona, J. Werner, B. Niesen, C. Ballif, M. Sessolo, H.J. Bolink, Efficient monolithic perovskite/perovskite tandem solar cells, *Adv. Energy Mater.* 7 (8) (2017), 1602121, <https://doi.org/10.1002/aenm.201602121>.
- J. Cao, C. Yan, C. Luo, W. Li, X. Zeng, Z. Xu, X. Fu, Q. Wang, X. Chu, H. Huang, X. Zhao, J. Lu, W. Yang, Cryogenic-temperature thermodynamically suppressed and strongly confined CsPbBr₃ quantum dots for deeply blue light-emitting diodes, *Adv. Opt. Mater.* 9 (17) (2021), 2100300, <https://doi.org/10.1002/adom.202100300>.
- K. Lin, J. Xing, L.N. Quan, F.P.G. de Arquer, X. Gong, J. Lu, L. Xie, W. Zhao, D. Zhang, C. Yan, W. Li, X. Liu, Y. Lu, J. Kirman, E.H. Sargent, Q. Xiong, Z. Wei, Perovskite light-emitting diodes with external quantum efficiency exceeding 20 per cent, *Nature* 562 (7726) (2018) 245–248, <https://doi.org/10.1038/s41586-018-0575-3>.
- Y. Cao, N. Wang, H. Tian, J. Guo, Y. Wei, H. Chen, Y. Miao, W. Zou, K. Pan, Y. He, H. Cao, Y. Ke, M. Xu, Y. Wang, M. Yang, K. Du, Z. Fu, D. Kong, D. Dai, Y. Jin, G. Li, H. Li, Q. Peng, J. Wang, W. Huang, Perovskite light-emitting diodes based on spontaneously formed submicrometre-scale structures, *Nature* 562 (7726) (2018) 249–253, <https://doi.org/10.1038/s41586-018-0576-2>.
- J.Y. Lee, S.Y. Kim, H.J. Yoon, Small molecule approach to passivate undercoordinated ions in perovskite light emitting diodes: progress and challenges, *Adv. Opt. Mater.* 10 (1) (2021), 2101361, <https://doi.org/10.1002/adom.202101361>.
- S.Y. Kim, H. Kang, K. Chang, H.J. Yoon, Case studies on structure–property relations in perovskite light-emitting diodes via interfacial engineering with self-assembled monolayers, *ACS Appl. Mater. Interfaces* 13 (26) (2021) 31236–31247, <https://doi.org/10.1021/acsami.1c03797>.
- H. Zhang, T. Yu, C. Wang, R. Jia, A.A.A. Pirzado, D. Wu, X. Zhang, X. Zhang, J. Jie, High-luminance microsized CH₃NH₃PbBr₃ single-crystal-based light-emitting diodes via a facile liquid-insulator bridging route, *ACS Nano* 16 (4) (2022) 6394–6403, <https://doi.org/10.1021/acsnano.2c00488>.
- Y. Chen, H. Yang, J. Song, B. Zhang, An effective Fe(II) doping strategy for stable and highly photoluminescent CsPbBr₂ nanocrystals, *J. Mater. Chem. C* 10 (13) (2022) 5147–5154, <https://doi.org/10.1039/D1TC05831B>.
- S.Y. Kim, S.J. Cho, S.E. Byeon, X. He, H.J. Yoon, Self-assembled monolayers as interface engineering nanomaterials in perovskite solar cells, *Adv. Energy Mater.* 10 (44) (2020), 2002606, <https://doi.org/10.1002/aenm.202002606>.
- H. Zhu, Y. Fu, F. Meng, X. Wu, Z. Gong, Q. Ding, M.V. Gustafsson, M.T. Trinh, S. Jin, X.Y. Zhu, Lead halide perovskite nanowire lasers with low lasing thresholds and high quality factors, *Nat. Mater.* 14 (6) (2015) 636–642, <https://doi.org/10.1038/nmat4271>.
- S.A. Veldhuis, P.P. Boix, N. Yantara, M. Li, T.C. Sum, N. Mathews, S.G. Mhaisalkar, Perovskite materials for light-emitting diodes and lasers, *Adv. Mater.* 28 (32) (2016) 6804–6834, <https://doi.org/10.1002/adma.201600669>.
- Y.C. Kim, K.H. Kim, D.Y. Son, D.N. Jeong, J.Y. Seo, Y.S. Choi, I.T. Han, S.Y. Lee, N. G. Park, Printable organometallic perovskite enables large-area, low-dose X-ray imaging, *Nature* 550 (7674) (2017) 87–91, <https://doi.org/10.1038/nature24032>.
- Y. Zhang, R. Sun, X. Ou, K. Fu, Q. Chen, Y. Ding, L.J. Xu, L. Liu, Y. Han, A.V. Malko, X. Liu, H. Yang, O.M. Bakr, H. Liu, O.F. Mohammed, Metal halide perovskite nanosheet for X-ray high-resolution scintillation imaging screens, *ACS Nano* 13 (2) (2019) 2520–2525, <https://doi.org/10.1021/acsnano.8b09484>.
- L.N. Quan, B.P. Rand, R.H. Friend, S.G. Mhaisalkar, T.W. Lee, E.H. Sargent, Perovskites for next-generation optical sources, *Chem. Rev.* 119 (12) (2019) 7444–7477, <https://doi.org/10.1021/acs.chemrev.9b00107>.
- Q. Mo, C. Chen, W. Cai, S. Zhao, D. Yan, Z. Zang, Room temperature synthesis of stable zirconia-coated CsPbBr₃ nanocrystals for white light-emitting diodes and visible light communication, *Laser Photonics Rev.* 15 (10) (2021), 2100278, <https://doi.org/10.1002/lpor.202100278>.
- K. Lin, C. Yan, R.P. Sabatini, W. Feng, J. Lu, K. Liu, D. Ma, Y. Shen, Y. Zhao, M. Li, C. Tian, L. Xie, E.H. Sargent, Z. Wei, Dual-phase regulation for high-efficiency perovskite light-emitting diodes, *Adv. Funct. Mater.* 5 (13) (2022), 2200350, <https://doi.org/10.1002/adfm.202200350>.
- X.K. Liu, W. Xu, S. Bai, Y. Jin, J. Wang, R.H. Friend, F. Gao, Metal halide perovskites for light-emitting diodes, *Nat. Mater.* 20 (1) (2021) 10–21, <https://doi.org/10.1038/s41563-020-0784-7>.
- S.A. Kulkarni, N. Yantara, K.S. Tan, N. Mathews, S.G. Mhaisalkar, Perovskite nanostructures: leveraging quantum effects to challenge optoelectronic limits, *Mater. Today* 33 (2020) 122–140, <https://doi.org/10.1016/j.mattod.2019.10.021>.
- P. Du, J. Li, L. Wang, L. Sun, X. Wang, X. Xu, L. Yang, J. Pang, W. Liang, J. Luo, Y. Ma, J. Tang, Efficient and large-area all vacuum-deposited perovskite light-emitting diodes via spatial confinement, *Nat. Commun.* 12 (1) (2021) 4751, <https://doi.org/10.1038/s41467-021-25093-6>.
- X. Lian, X. Wang, Y. Ling, E. Lochner, L. Tan, Y. Zhou, B. Ma, K. Hanson, H. Gao, Light emitting diodes based on inorganic composite halide perovskites, *Adv. Funct. Mater.* 29 (5) (2019), 1807345, <https://doi.org/10.1002/adfm.201807345>.
- J. Li, P. Du, S. Li, J. Liu, M. Zhu, Z. Tan, M. Hu, J. Luo, D. Guo, L. Ma, Z. Nie, Y. Ma, L. Gao, G. Niu, J. Tang, High-throughput combinatorial optimizations of perovskite light-emitting diodes based on all-vacuum deposition, *Adv. Funct. Mater.* 29 (51) (2019), 1903607, <https://doi.org/10.1002/adfm.201903607>.
- L.N. Quan, R. Quintero-Bermudez, O. Voznyy, G. Walters, A. Jain, J.Z. Fan, X. Zheng, Z. Yang, E.H. Sargent, Highly emissive green perovskite nanocrystals in a solid state crystalline matrix, *Adv. Mater.* 29 (21) (2017), 1605945, <https://doi.org/10.1002/adma.201605945>.
- Z. Bao, Y.J. Tseng, W. You, W. Zheng, X. Chen, S. Mahlik, A. Lazarowska, T. Lesniewski, M. Grinberg, C. Ma, W. Sun, W. Zhou, R.S. Liu, J.P. Attfield, Efficient luminescence from CsPbBr₃ nanoparticles embedded in Cs₄PbBr₆, *J. Phys. Chem. Lett.* 11 (18) (2020) 7637–7642, <https://doi.org/10.1021/acs.jpclett.0c02321>.
- J. Xu, W. Huang, P. Li, D.R. Onken, C. Dun, Y. Guo, K.B. Ucer, C. Lu, H. Wang, S. M. Geyer, R.T. Williams, D.L. Carroll, Imbedded nanocrystals of CsPbBr₃ in Cs₄PbBr₆: kinetics, enhanced oscillator strength, and application in light-emitting diodes, *Adv. Mater.* 29 (43) (2017), 1703703, <https://doi.org/10.1002/adma.201703703>.
- Q. He, E. Mei, X. Liang, W. Xiang, Ultrastable PVB films-protected CsPbBr₃/Cs₄PbBr₆ perovskites with high color purity for near-infrared, *Chem. Eng. J.* 419 (2021), 129529, <https://doi.org/10.1016/j.cej.2020.129529>.
- X. Chen, F. Zhang, Y. Ge, L. Shi, S. Huang, J. Tang, Z. Lv, L. Zhang, B. Zou, H. Zhong, Centimeter-sized Cs₄PbBr₆ crystals with embedded CsPbBr₃ nanocrystals showing superior photoluminescence: nonstoichiometry induced transformation and light-emitting applications, *Adv. Funct. Mater.* 28 (16) (2018), 1706567, <https://doi.org/10.1002/adfm.201706567>.
- G. Kaur, K.J. Babu, N. Ghorai, T. Goswami, S. Maiti, H.N. Ghosh, Polaron-mediated slow carrier cooling in a type-1 3D/0D CsPbBr₃@Cs₄PbBr₆ core-shell perovskite system, *J. Phys. Chem. Lett.* 10 (18) (2019) 5302–5311, <https://doi.org/10.1021/acs.jpclett.9b01552>.
- G. Jiang, C. Guhrenz, A. Kirch, L. Sonntag, C. Bauer, X. Fan, J. Wang, S. Reineke, N. Gaponik, A. Eychmüller, Highly luminescent and water-resistant CsPbBr₃-CsPbBr₃ perovskite nanocrystals coordinated with partially hydrolyzed poly(methyl methacrylate) and polyethylenimine, *ACS Nano* 13 (9) (2019) 10386–10396, <https://doi.org/10.1021/acsnano.9b04179>.
- P.R. Huang, B. Ma, H. Wang, N. Li, R.T. Liu, Z.Q. Zhang, X.D. Zhang, J.H. Zhao, P. Z. Zheng, Q. Wang, H.L. Zhang, *In situ* growth of 3D/2D (CsPbBr₃/CsPb₂Br₅) perovskite heterojunctions toward optoelectronic devices, *J. Phys. Chem. Lett.* 11 (15) (2020) 6007–6015, <https://doi.org/10.1021/acs.jpclett.0c01757>.
- X. Sun, X. Shi, W. Zhang, B. Xu, Z. Gao, Z. Wang, X. Wang, X. Meng, 2D/3D heterostructure derived from phase transformation of 0D perovskite for random lasing applications with remarkably improved water resistance, *Nanoscale* 13 (44) (2021) 18647–18656, <https://doi.org/10.1039/D1NR06084H>.
- D. Baranov, G. Caputo, L. Goldoni, Z. Dang, R. Scarfello, L. De Trizio, A. Portone, F. Fabbri, A. Camposco, D. Pisignano, L. Manna, Transforming colloidal Cs₄PbBr₆ nanocrystals with poly(maleic anhydride-alt-1-octadecene) into stable CsPbBr₃ perovskite emitters through intermediate heterostructures, *Chem. Sci.* 11 (15) (2020) 3986–3995, <https://doi.org/10.1039/D0SC00738B>.
- Y.M. Chen, Y. Zhou, Q. Zhao, J.Y. Zhang, J.P. Ma, T.T. Xuan, S.Q. Guo, Z.J. Yong, J. Wang, Y. Kuroiwa, C. Moriyoshi, H.T. Sun, Cs₄PbBr₆/CsPbBr₃ perovskite composites with near-unity luminescence quantum yield: large-scale synthesis, luminescence and formation mechanism, and white light-emitting diode application, *ACS Appl. Mater. Interfaces* 10 (18) (2018) 15905–15912, <https://doi.org/10.1021/acsami.8b04556>.
- L.N. Quan, Y. Zhao, F.P. García de Arquer, R. Sabatini, G. Walters, O. Voznyy, R. Comin, Y. Li, J.Z. Fan, H. Tan, J. Pan, M. Yuan, O.M. Bakr, Z. Lu, D.H. Kim, E. H. Sargent, Tailoring the energy landscape in Quasi-2D halide perovskites enables efficient green-light emission, *Nano Lett.* 17 (6) (2017) 3701–3709, <https://doi.org/10.1021/acs.nanolett.7b00976>.

- [36] C. Zhang, S. Wang, X. Li, M. Yuan, L. Turyanska, X. Yang, Core/shell perovskite nanocrystals: synthesis of highly efficient and environmentally stable FAPbBr₃/CsPbBr₃ for LED applications, *Adv. Funct. Mater.* 30 (31) (2020), 1910582, <https://doi.org/10.1002/adfm.201910582>.
- [37] K.K. Liu, Q. Liu, D.W. Yang, Y.C. Liang, L.Z. Sui, J.Y. Wei, G.W. Xue, W.B. Zhao, X. Y. Wu, L. Dong, C.X. Shan, Water-induced MAPbBr₃@PbBr(OH) with enhanced luminescence and stability, *Light Sci. Appl.* 9 (1) (2020) 44, <https://doi.org/10.1038/s41377-020-0283-2>.
- [38] X. Zhang, X. Bai, H. Wu, X. Zhang, C. Sun, Y. Zhang, W. Zhang, W. Zheng, W.W. Yu, A.L. Rogach, Water-assisted size and shape control of CsPbBr₃ perovskite nanocrystals, *Angew. Chem. Int. Ed.* 57 (13) (2018) 3337–3342, <https://doi.org/10.1002/anie.201710869>.
- [39] F. Fang, W. Chen, Y. Li, H. Liu, M. Mei, R. Zhang, J. Hao, M. Mikita, W. Cao, R. Pan, K. Wang, X.W. Sun, Employing polar solvent controlled ionization in precursors for synthesis of high-quality inorganic perovskite nanocrystals at room temperature, *Adv. Funct. Mater.* 28 (10) (2018), 1706000, <https://doi.org/10.1002/adfm.201706000>.
- [40] M. Liu, S.K. Matta, H. Ali-Löyty, A. Matuhina, G.K. Grandhi, K. Lahtonen, S. P. Russo, P. Vivo, Moisture-assisted near-UV emission enhancement of lead-free Cs₄CuIn₂Cl₁₂ double perovskite nanocrystals, *Nano Lett.* 22 (1) (2022) 311–318, <https://doi.org/10.1021/acs.nanolett.1c03822>.
- [41] Y. Su, Q. Zeng, X. Chen, W. Ye, L. She, X. Gao, Z. Ren, X. Li, Highly efficient CsPbBr₃ perovskite nanocrystals induced by structure transformation between CsPbBr₃ and Cs₄PbBr₆ phases, *J. Mater. Chem. C* 7 (25) (2019) 7548–7553, <https://doi.org/10.1039/C9TC01763A>.
- [42] D. Di Girolamo, M.I. Dar, D. Dini, L. Gontrani, R. Caminiti, A. Mattoni, M. Graetzel, S. Meloni, Dual effect of humidity on cesium lead bromide: enhancement and degradation of perovskite films, *J. Mater. Chem. A* 7 (19) (2019) 12292–12302, <https://doi.org/10.1039/C9TA00715F>.
- [43] S. Cheng, H. Zhong, What happens when halide perovskites meet with water? *J. Phys. Chem. Lett.* 13 (10) (2022) 2281–2290, <https://doi.org/10.1021/acs.jpcclett.2c00166>.
- [44] A.M.A. Leguy, Y. Hu, M. Campoy-Quiles, M.I. Alonso, O.J. Weber, P. Azarhoosh, M. van Schilfgaarde, M.T. Weller, T. Bein, J. Nelson, P. Docampo, P.R.F. Barnes, Reversible hydration of CH₃NH₃PbI₃ in films, single crystals, and solar cells, *Chem. Mater.* 27 (9) (2015) 3397–3407, <https://doi.org/10.1021/acs.chemmater.5b00660>.
- [45] Y. Liu, L.K. Ono, G. Tong, H. Zhang, Y. Qi, Two-dimensional dion-jacobson structure perovskites for efficient sky-blue light-emitting diodes, *ACS Energy Lett.* 6 (3) (2021) 908–914, <https://doi.org/10.1021/acsenergylett.1c00129>.
- [46] N. Loganathan, A.O. Yazaydin, G.M. Bowers, A.G. Kalinichev, R.J. Kirkpatrick, Structure, energetics, and dynamics of Cs⁺ and H₂O in hectorite: molecular dynamics simulations with an unconstrained substrate surface, *J. Phys. Chem. C* 120 (19) (2016) 10298–10310, <https://doi.org/10.1021/acs.jpcc.6b01016>.
- [47] X. Li, B. Kang, F. Dong, Z. Zhang, X. Luo, L. Han, J. Huang, Z. Feng, Z. Chen, J. Xu, B. Peng, Z.L. Wang, Enhanced photocatalytic degradation and H₂/H₂O₂ production performance of S-pCN/WO_{2.72} S-scheme heterojunction with appropriate surface oxygen vacancies, *Nano Energy* 81 (2021), 105671, <https://doi.org/10.1016/j.nanoen.2020.105671>.
- [48] Q. Zhang, X. Sun, W. Zheng, Q. Wan, M. Liu, X. Liao, T. Hagio, R. Ichino, L. Kong, H. Wang, L. Li, Band gap engineering toward wavelength tunable CsPbBr₃ nanocrystals for achieving Rec. 2020 displays, *Chem. Mater.* 33 (10) (2021) 3575–3584, <https://doi.org/10.1021/acs.chemmater.1c00145>.
- [49] N. Mondal, A. De, A. Samanta, Achieving near-unity photoluminescence efficiency for blue-violet-emitting perovskite nanocrystals, *ACS Energy Lett.* 4 (1) (2019) 32–39, <https://doi.org/10.1021/acseenergylett.8b01909>.
- [50] J.N. Yang, T. Chen, J. Ge, J.J. Wang, Y.-C. Yin, Y.F. Lan, X.C. Ru, Z.Y. Ma, Q. Zhang, H.B. Yao, High color purity and efficient green light-emitting diode using perovskite nanocrystals with the size overly exceeding bohr exciton diameter, *J. Am. Chem. Soc.* 143 (47) (2021) 19928–19937, <https://doi.org/10.1021/jacs.1c09948>.
- [51] F. Zhang, H. Zhong, C. Chen, X.G. Wu, X. Hu, H. Huang, J. Han, B. Zou, Y. Dong, Brightly luminescent and color-tunable colloidal CH₃NH₃PbX₃ (X = Br, I, Cl) quantum dots: potential alternatives for display technology, *ACS Nano* 9 (4) (2015) 4533–4542, <https://doi.org/10.1021/acs.nano.5b01154>.
- [52] B.J. Moon, S.J. Kim, S. Lee, A. Lee, H. Lee, D.S. Lee, T.W. Kim, S.K. Lee, S. Bae, S. H. Lee, Rare-earth-element-ytterbium-substituted lead-free inorganic perovskite nanocrystals for optoelectronic applications, *Adv. Mater.* 31 (33) (2019), 1901716, <https://doi.org/10.1002/adma.201901716>.
- [53] J. Zhang, Y. Yang, H. Deng, U. Farooq, X.K. Yang, J. Khan, J. Tang, H.S. Song, High quantum yield blue emission from lead free inorganic antimony halide perovskite colloidal quantum dots, *ACS Nano* 11 (9) (2017) 9294–9302.